

## EARTH SCIENCES

<sup>1</sup>Geophysical Institute, University of Bergen and Bjerknes Center for Climate Research, Bergen 5007, Norway; <sup>2</sup>Key Laboratory of Meteorological Disaster/Collaborative Innovation Center on Forecast and Evaluation of Meteorological Disasters, Nanjing University of Information Science and Technology, Nanjing 210044, China; <sup>3</sup>Climate Change Research Center, Chinese Academy of Sciences, Beijing 100029, China; <sup>4</sup>Nansen-Zhu International Research Centre, Institute of Atmospheric Physics, Chinese Academy of Sciences, Beijing 100029, China; <sup>5</sup>Norwegian Institute for Air Research, Kjeller 2007, Norway and <sup>6</sup>State Key Laboratory of Space Weather, National Space Science Center, Chinese Academy of Sciences, Beijing 100190, China


\*Corresponding author. E-mail: [Shengping.He@uib.no](mailto:Shengping.He@uib.no)

Received 16 December 2018;

Revised 8 April 2019;

Accepted 21 June 2019

# Solar-wind–magnetosphere energy influences the interannual variability of the northern-hemispheric winter climate

Shengping He <sup>1,2,3,\*</sup>, Huijun Wang<sup>2,3,4</sup>, Fei Li<sup>5,2,4</sup>, Hui Li<sup>6</sup> and Chi Wang<sup>6</sup>

## ABSTRACT

Solar irradiance has been universally acknowledged to be dominant by quasi-decadal variability, which has been adopted frequently to investigate its effect on climate decadal variability. As one major terrestrial energy source, solar-wind energy flux into Earth's magnetosphere ( $E_{in}$ ) exhibits dramatic interannual variation, the effect of which on Earth's climate, however, has not drawn much attention. Based on the  $E_{in}$  estimated by 3D magnetohydrodynamic simulations, we demonstrate a novelty that the annual mean  $E_{in}$  can explain up to 25% total interannual variance of the northern-hemispheric temperature in the subsequent boreal winter. The concurrent anomalous atmospheric circulation resembles the positive phase of Arctic Oscillation/North Atlantic Oscillation. The warm anomalies in the tropic stratopause and tropopause induced by increased solar-wind–magnetosphere energy persist into the subsequent winter. Due to the dominant change in the polar vortex and mid-latitude westerly in boreal winter, a 'top-down' propagation of the stationary planetary wave emerges in the Northern Hemisphere and further influences the atmospheric circulation and climate.

**Keywords:** solar wind, winter climate, interannual variability, stratosphere

## INTRODUCTION

As the fundamental energy source of Earth's climate, the solar irradiance can dramatically influence Earth's climate, the earliest study of which can be traced back to the early eighteenth century [1]. It is well recognized that the variability of the solar activity (e.g. sunspot number, solar radio flux at 10.7 cm) exhibits mainly the quasi-decadal variability (i.e. prominent 11-year cycle) [2–4]. In the past >100 years, there has been a growing body of evidence that the tropospheric and stratospheric climatic variables are affected by the solar activity on both global and regional scales [5–10].

In the stratosphere, the heating can be modulated by the solar cycle due to the variations in the ultraviolet absorption by ozone [11,12]. Associated with the solar maximum, the upper stratospheric zonally averaged temperature at the equator, where the solar radiative input is the largest [13], is higher compared to that at the solar minimum [14]. The

increase in solar radiative input during the solar maximum can lead to 1–2°C of increasing in the zonal-mean annual temperature located below the equatorial stratopause [15,16]. Such positive temperature anomalies intensify the mean poleward meridional temperature gradient and hence lead to anomalous westerly wind at mid-latitudes of the Northern Hemisphere [17,18]. As the propagation of the planetary waves has close relation to the background zonal winds, a downward propagation of the atmospheric anomaly to mid- and high latitudes of the lower stratosphere is generally observed at the solar maximum [13,18,19]. Such a stratosphere 'top-down' influence provides a potential pathway through which the solar cycle influences the interdecadal variability of the tropospheric circulation and climate in the Northern Hemisphere.

It should be noted that most of the previous studies have adopted the parameters that are dominated by quasi-decadal (i.e. 11-year-cycle)

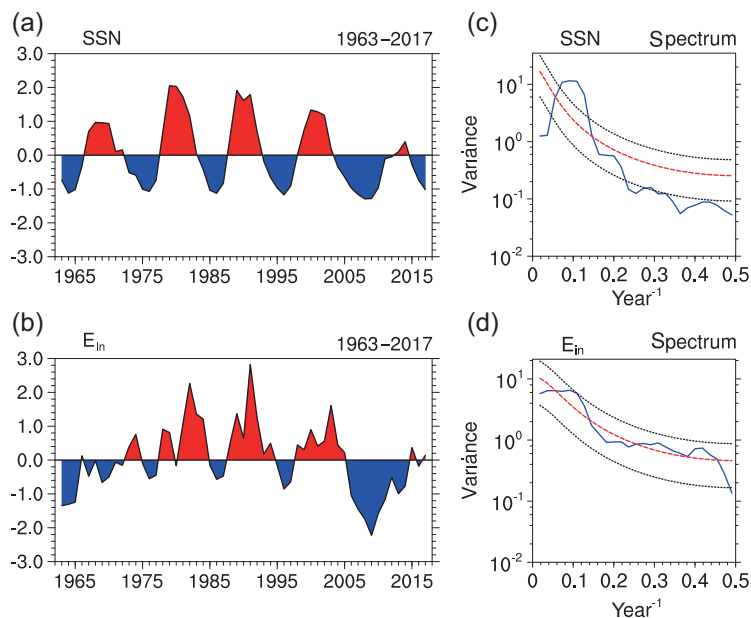


**Figure 1.** Decadal and interannual variability of solar variables. Normalized time series of annual mean (a) SSN, (b)  $E_{in}$  during 1963–2017. Spectral analysis (blue curves) for (c) SSN and (d)  $E_{in}$ ; the red dashed line indicates the red-noise confidence interval and the black dashed lines indicate the upper and lower confidence bounds.

variability, to investigate the solar impacts on the atmospheric circulation and climate. Such solar cycle–atmosphere/climate relationships are not a simple linear correlation on an interannual time scale, but rather a kind of decadal modulation effect of the 11-year solar cycle. For example, by comparing the solar-maximum with the solar-minimum periods, many studies have explored the different responses of the climate or investigated the different climatic impacts of other factors such as El Niño–Southern Oscillation (ENSO) [20,21], Arctic Oscillation [22,23] and North Atlantic Oscillation [24]. Actually, except for the quasi-decadal variability, higher-frequency variability also exists in solar activity [25]. It is estimated that the energy of the solar wind and cosmic rays can be increased by tens and hundreds of times during solar-maximum periods [26]. Therefore, it is very important to examine the potential influence of total energy input from the solar wind into Earth’s magnetosphere ( $E_{in}$ ) on the interannual variability of climate, which has been rarely discussed before due to the large challenge in quantitative estimation of  $E_{in}$  [27–29]. Utilizing the  $E_{in}$  quantitatively estimated by 3D magnetohydrodynamics (see the ‘DATA AND METHODS’ section) [30], in this study, we reveal a novel influence of solar-wind–magnetosphere energy on the winter climate over the Northern Hemisphere.

## SOLAR-WIND–MAGNETOSPHERE ENERGY IS LINKED TO NORTHERN-HEMISPHERIC WINTER TEMPERATURE AND ATMOSPHERIC CIRCULATION

The sunspot number (SSN) shows apparent low-frequency variability with alternate positive and negative phases during which no apparent high-frequency variability is observed (Fig. 1a). Even though alternate positive and negative phases are also observed in  $E_{in}$ , there is obvious high-frequency variability during positive/negative phases (Fig. 1b). To illustrate clearly the time scale of the variability, we present, in Fig. 1c and d, the spectral analysis of the time series. The results indicate that the SSN is dominated by decadal variability (Fig. 1c), while the  $E_{in}$  displays both interannual and decadal variability (Fig. 1d). Therefore, it is possible to investigate the interannual relationship between the  $E_{in}$  and the atmospheric circulation and climate.

Figure 2a indicates that, during the winters following higher  $E_{in}$  in the preceding year, significantly warmer anomalies extend from northwest Europe through Siberia to northeast Asia and cross from Alaska to southwest Canada, with a maximum amplitude of up to  $0.9^{\circ}\text{C}$  over Eurasia. Meanwhile, significantly colder anomalies emerge in south Europe (south of  $45^{\circ}\text{N}$ ) and East Canada to Greenland, with a maximum amplitude of up to  $-0.8^{\circ}\text{C}$ . The significant lag-relationship (with maximum correlation coefficients up to 0.5) indicates the possible forcing of solar-wind–magnetosphere energy to the northern-hemispheric winter climate. The results derived from the GISTEMP Team [31] resemble those derived from NCEP/NCAR reanalysis (Fig. 2b vs. a), with a spatial correlation of 0.78. It should be noted that the results will not show much difference when the linear influence of ENSO has been removed (not shown).

Boreal winter large-scale atmospheric circulation following higher-than-normal solar-wind–magnetosphere energy is further explored. As shown in Fig. 2c, corresponding to higher-than-normal annual mean  $E_{in}$ , the winters in subsequent years generally see significant positive sea-level-pressure (SLP) anomalies at mid-latitudes of the North Atlantic, with the maximum anomaly of 2.4 hPa at the central Atlantic (around  $45^{\circ}\text{N}$ ). The positive SLP anomalies extend across North America through the North Atlantic eastward to the Eurasian continent. At the same time, significant negative SLP anomalies are located in the Atlantic–Arctic sector, with minimum values of  $-2.4$  hPa centered at the Barents Sea. The spatial distribution of the winter SLP anomalies related to the higher-than-normal  $E_{in}$

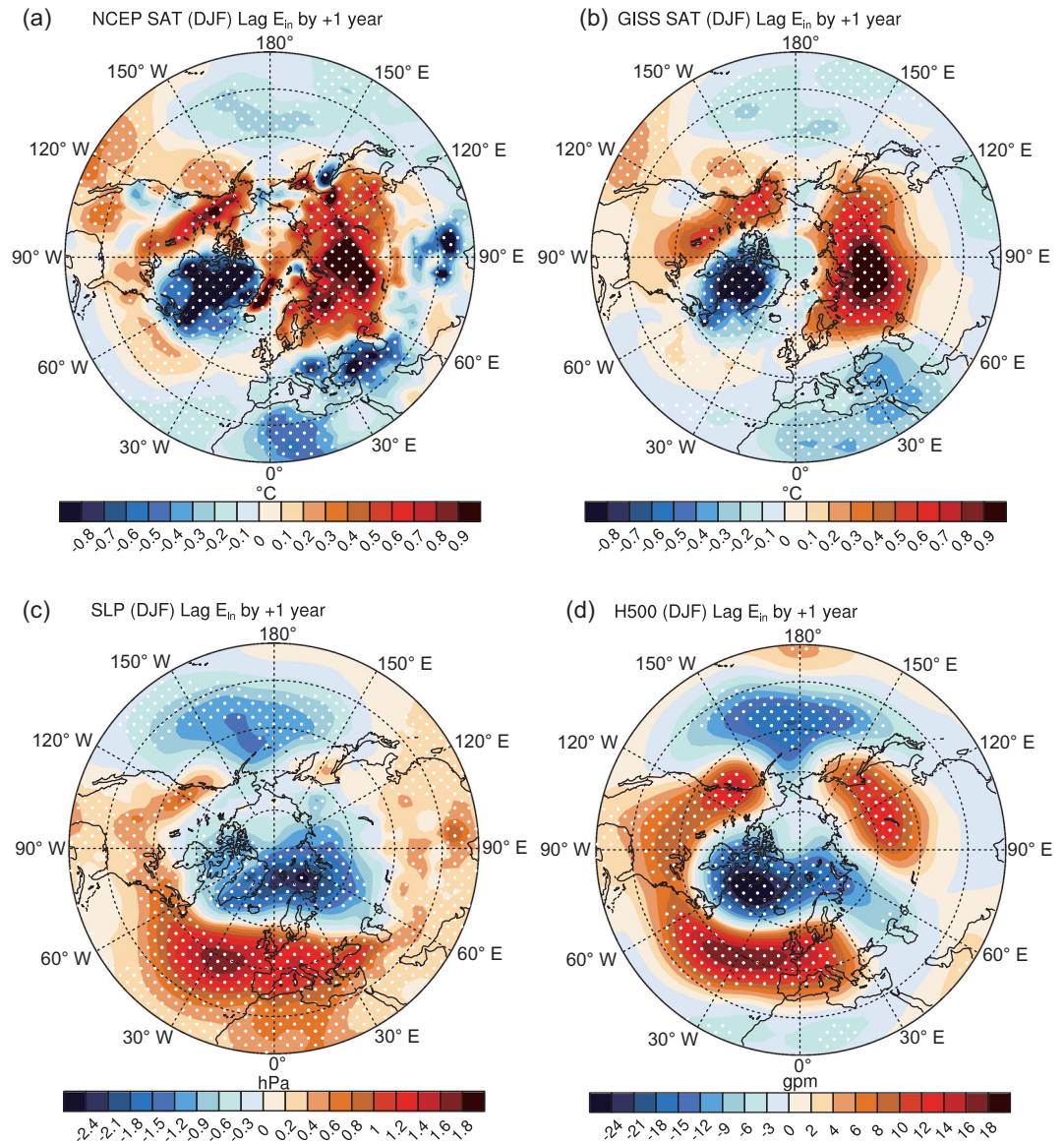


**Figure 2.** Lag relationship of boreal winter atmosphere with solar-wind energy. (a) Regression maps of surface air temperature north of 20°N during winter (December, January and February) 1964–2017 onto the normalized preceding annual mean of solar-wind energy flux into Earth's magnetosphere ( $E_{in}$ ) index during 1963–2016. Surface air temperature derives from NCEP/NCAR reanalysis. Dotted values are significant at the 90% confidence levels. (b) is the same as (a), but the surface air temperature derives from National Aeronautics and Space Administration, Goddard Institute for Space Studies (<http://data.giss.nasa.gov/gistemp/>). (c) and (d) are the same as (a), but for the sea-level pressure and 500-hPa geopotential height.

in the preceding year resemble the positive-phase North Atlantic Oscillation (NAO) or Arctic Oscillation (AO) pattern. A similar NAO-/AO-like pattern is also found in the 500-hPa geopotential height anomalies (Fig. 2d). Note that there is an additional significant positive anomaly center located over the Baikal, which is missing in the SLP field, indicating the possible ‘top-down’ propagated influence of solar-wind–magnetosphere energy. Results based on the interannual variability obtained from another

filtering method [32] are similar (Supplementary Fig. 1). The spatial pattern of the temperature anomalies related to the positive phase of AO/NAO (Supplementary Fig. 2a and c) resembles closely the one related to the higher-than-normal  $E_{in}$  (e.g. the spatial correlations of Fig. 2a with Supplementary Fig. 2a and b are 0.81 and 0.86, respectively). It further supports speculation that the significant interannual relationship between the solar-wind–magnetosphere energy and northern-hemispheric

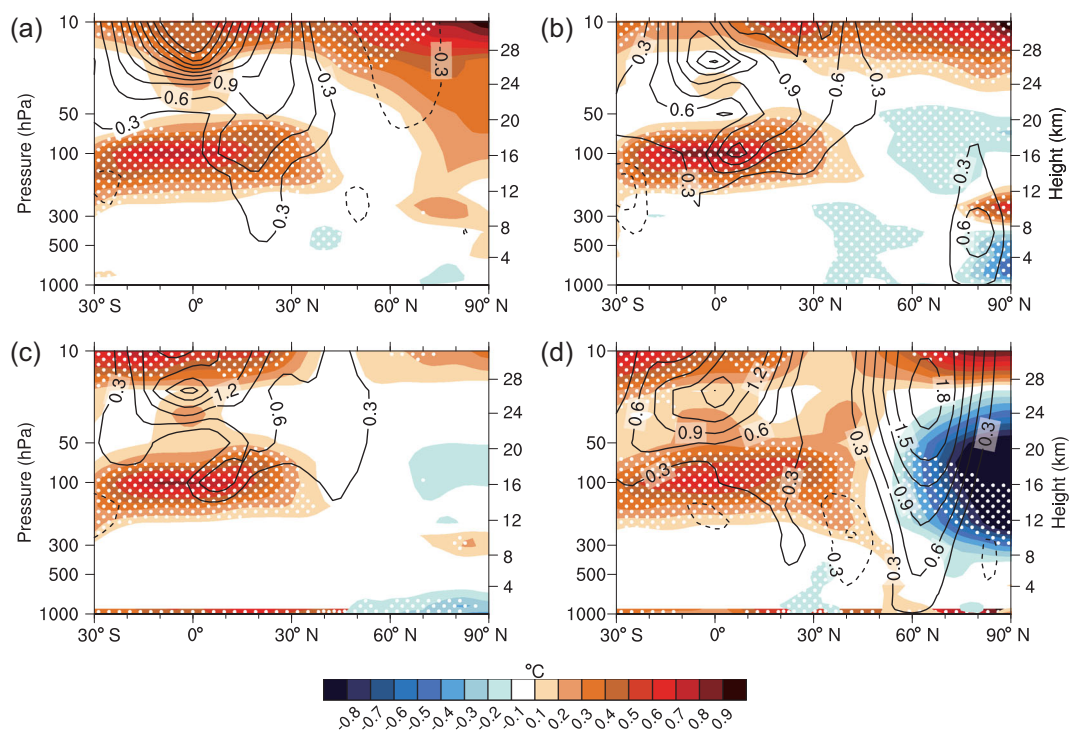


**Figure 3.** Persistence of anomalous signals in the atmosphere. Regression of zonally averaged zonal wind (contours) and air temperature (shading) in (a) March–May, (b) July–August, (c) September–November and (d) December–February during 1964–2017 onto the normalized preceding annual mean of solar-wind energy flux into Earth’s magnetosphere ( $E_{in}$ ) index during 1963–2016. Stippled regions indicate that the temperature anomalies are significant at the 90% confidence level from a two-tailed Student’s  $t$ -test.

winter climate may be attributed to the solar impacts on the NAO-/AO-related atmospheric circulation variability (Supplementary Fig. 3).

### STRATOSPHERIC–TROPOSPHERIC DYNAMICAL ANALYSES

Following the increase in solar-wind–magnetosphere energy, two statistically significant warming centers over the tropical region ( $30^{\circ}\text{S}$ – $30^{\circ}\text{N}$ ) with magnitude of up to  $0.5^{\circ}\text{C}$  emerge in the upper troposphere ( $200$ – $70$  hPa  $\approx 12$ – $18$  km) and stratopause, persisting from boreal spring (March to April) to boreal winter (Fig. 3a–d, shading). The two warming responses might be caused by the increased solar ultraviolet irradiance and adiabatic warming as well as increased ozone heating [33,34]. In boreal winter, the higher solar-wind–magnetosphere energy intensifies dramatically the stratospheric polar vortex [19] (Supplementary Fig. 4). Due to the intensification of the polar vortex, a dominant cooling of  $-0.9^{\circ}\text{C}$  emerges in the upper troposphere and lower stratosphere over the polar region (Fig. 3d, shading). Consequently, the poleward temperature

gradient is further intensified in boreal winter, which induces an apparent westerly-wind anomaly at high latitudes with maximum acceleration in the speed of up to  $1.8\text{ m s}^{-1}$  (around  $60^{\circ}\text{N}$ ; Fig. 3d, contours). Note that the interannual variability of the zonal-mean air temperature, high-latitude zonal wind and polar vortex in boreal winter at lag +1 year responding to the  $E_{in}$  is in good agreement with the counterparts of the solar maximum revealed by Thiéblemont *et al.* [19]. It implies that the previously proposed pathway, on a decadal time scale, can also link the solar activity to the northern-hemispheric climate on an interannual time scale. Great potentials of impacts and applications could be explored from the solar-wind–magnetosphere energy.

Anomalous zonal background flow can alter the planetary-wave propagation from the stratosphere downward to the troposphere so as to connect the solar signals with the surface climate in boreal winter [35]. When there is higher annual mean solar-wind–magnetosphere energy, the subsequent years’ winters experience apparent anomalous E–P fluxes propagating from the upper stratosphere downward into the troposphere at latitudes north of  $60^{\circ}\text{N}$  (Supplementary Fig. 5a, vectors). The anomalous

downward propagations of the winter E–P flux may be induced by the acceleration of the high-latitude westerly wind in winter (Fig. 3d, contours), which is unfavorable for the upward propagation of planetary waves [36]. The anomalous downward-propagating planetary waves lead to E–P flux divergence anomalies in the stratosphere and upper troposphere at high latitudes (Supplementary Fig. 5, shading), which further accelerates the westerly wind and strengthens the polar vortex (Supplementary Fig. 4, shading) [35,37,38]. Such a mean flow-wave interaction in the stratosphere may provide one possible way to maintain the downward propagation of the solar signals [19]. It may be noted that apparent planetary waves propagate from the lower troposphere at mid-latitudes (between 30° and 60°N) upwards to the upper troposphere (~100 hPa) and bend equator-ward (Supplementary Fig. 5, vectors), which may be induced by the mid-latitude sea-surface temperature anomalies related to the solar-wind–magnetosphere energy [19]. Because equatorward-pointing E–P fluxes correspond to poleward meridional eddy momentum flux, the increase in solar-wind–magnetosphere energy induces eddy westerly momentum flux anomalies toward to the Arctic from the middle to upper troposphere (Supplementary Fig. 5, vectors between 300 and 100 hPa). These poleward-momentum fluxes further help to sustain the anomalous westerly at high latitudes (north 60°N), causing the downward migration of the westerly anomaly from the stratosphere downward to the troposphere so as to impact tropospheric circulation. Such a mean flow-wave interaction in the troposphere favors the influence of solar-wind–magnetosphere energy on the tropospheric circulation and climate.

The downward-propagating winter atmospheric anomalies related to the solar-wind–magnetosphere energy variability is very clearly seen by inspecting the geopotential height anomalies. The geopotential height in subtropics of the North Atlantic, Eurasian continent and North America shows a significant increase in anomalies from the upper troposphere to the stratosphere during spring, summer and autumn (figures not shown). By the winter, the positive geopotential height anomalies propagate from the stratosphere downwards to the lower troposphere at mid-latitudes (Fig. 4a–c), which is most apparent over the North Atlantic (Fig. 4a). The dominant downward-propagating geopotential height anomalies at mid-latitudes in boreal winter may be related to the Brewer–Dobson circulation, which is most active in boreal winter [39,40]. Concurrently with the changes in the geopotential height, significant westerly anomalies propagate from the stratosphere downwards to the lower troposphere at high lati-

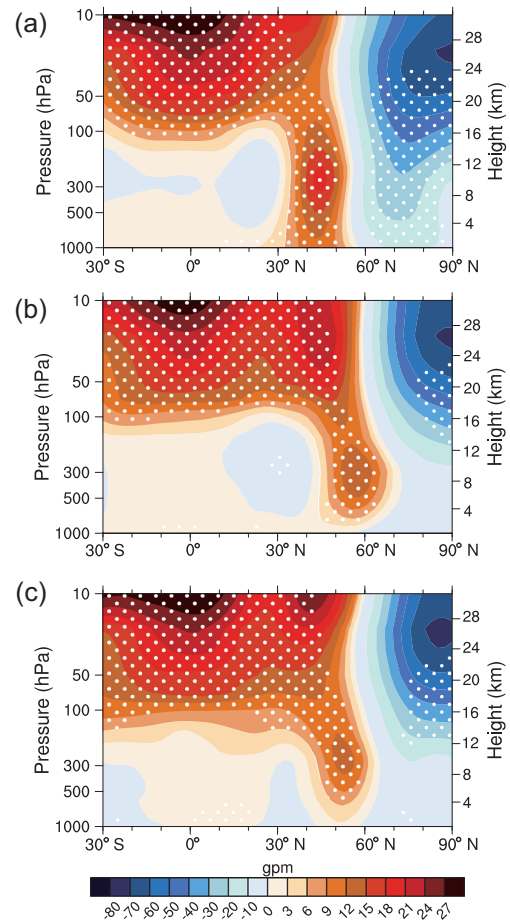


**Figure 4.** ‘Top-down’ propagation of atmospheric anomalies. Vertical–horizontal cross-section for geopotential height anomalies (shading) averaged along (a) 60°W–0°, (b) 90°E–150°E and (c) 150°W–90°W during 1964–2017 winters onto the normalized preceding annual mean of solar-wind energy flux into Earth’s magnetosphere ( $E_{in}$ ) index during 1963–2016. Stippled regions indicate that the anomalies are significant at the 90% confidence level from a two-tailed Student’s *t*-test.

tudes (around 60°N) (Supplementary Fig. 6a–c). Daily geopotential height anomalies also indicate that the significant positive height anomalies are located in the subtropical stratosphere before the end of November and start to propagate downwards to the troposphere at the end of November (Supplementary Fig. 7).

Consequently, two Rossby-wave-like patterns are observed in the troposphere: one propagates from the North Pacific to North America and the other propagates from the North Atlantic eastward to Eurasia (Supplementary Fig. 8a–c, vectors). The schematic is illustrated in Fig. 5. The horizontal propagation of Rossby waves can influence the blocking frequency and therefore affect the winter climate over the Northern Hemisphere [41]. The frequency of winter Ural blocking is reduced

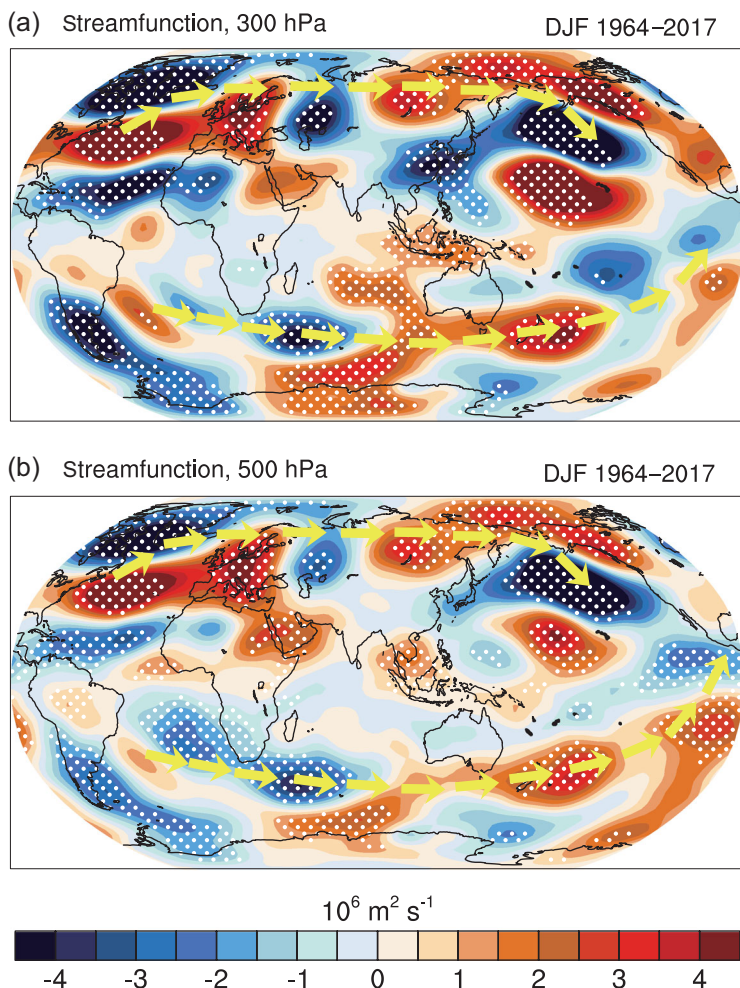


**Figure 5.** Schematic horizontal propagation of atmospheric teleconnection. Composite of stream-function anomalies at (a) 300 hPa and (b) 500 hPa between the winters (1982, 1983, 1984, 1985, 1990, 1992, 1993, 2004) following higher-than-normal annual  $E_{in}$  and those (1964, 1965, 1966, 2008, 2009, 2010, 2011, 2012) following lower-than-normal annual  $E_{in}$  in 1963–2016. Stippled values are significant at the 90% confidence levels. The yellow arrows show schematically the main wave trains emanating for the North and South Atlantic.

significantly by over 30% corresponding to one standard deviation of increase in the annual mean  $E_{in}$  in the preceding year (Supplementary Fig. 9a). As a result, the winter extreme cold (warm) days are significantly decreased (increased) over northern Eurasia (Supplementary Fig. 9b and c). Meanwhile, the winter blocking frequency is increased by over 25% from North America to north Europe and decreased by over 35% from north Canada to Greenland (Supplementary Fig. 9a). The significant anomalies of the blocking frequency, extremely cold days and extremely warm days in winter can explain well the anomalous winter climate over the Northern Hemisphere that is induced by the solar-wind–magnetosphere energy variability.

## CONCLUSIONS

Recent analyses of the solar/atmosphere relationship conducted by comparing two multi-decadal ocean–atmosphere chemistry–climate simulations with and without solar-forcing variability revealed a significant response of the boreal winter atmosphere at lag +1 year to the decadal variability (i.e. the 11-year solar cycle) [19]. However, the interannual relationship between the solar activity and the northern-hemispheric climate has not drawn much attention.

Based on a new index estimated by 3D magneto-hydrodynamic simulations, this study reveals a novel statistically significant interannual relationship between the annual mean  $E_{in}$  and the following boreal winter climate over the Northern Hemisphere. The high variance (up to 25%, i.e.  $r^2 = 0.25$ ) of winter SAT over the Northern Hemisphere explained by the preceding year’s solar-wind–magnetosphere energy sheds a promising improvement on climate predictions. It suggests that not only the quasi-decadal variability, but also the interannual variability of solar activity should be taken into account in climate prediction.

## DATA AND METHODS

### Energy input from the solar wind into the Earth’s magnetosphere ( $E_{in}$ ) and atmospheric variables

The  $E_{in}$  (units: W) is estimated quantitatively using a 3D magnetohydrodynamic simulation [30]:

$$E_{in} = 3.78 \times 10^7 n_{SW}^{0.24} V_{SW}^{1.47} B_T^{0.86} \times \left[ \sin^{2.70} \left( \frac{\theta}{2} \right) + 0.25 \right].$$

Here,  $n_{SW}$  and  $V_{SW}$  are the solar-wind number density (units:  $\text{cm}^{-3}$ ) and solar-wind velocity (units:  $\text{km s}^{-1}$ ), respectively;  $B_T$  is the transverse magnetic-field magnitude (units: nT); and  $\theta$  is the interplanetary magnetic-field clock angle. Solar-wind data were obtained from OMNIweb (<http://omniweb.gsfc.nasa.gov/>) of Goddard Space Flight Center in National Aeronautics and Space Administration (NASA). Wang *et al.* [30] suggested that the  $E_{in}$  shows good performance in quantitatively estimating the energy input on a global scale.

Monthly mean and daily mean atmospheric variables were obtained from National Centers for Environmental Prediction–National Center for Atmospheric Research (NCEP/NCAR) reanalysis [42]. The monthly mean surface temperature from

the Goddard Institute for Space Studies in NASA [31] was employed to support the results derived from the NCEP/NCAR reanalysis.

### Extreme events

An extremely cold/warm day is defined when a daily maximum temperature is lower (higher) than the 10<sup>th</sup> (90<sup>th</sup>) percentile value [43]. The 10<sup>th</sup> and 90<sup>th</sup> percentile values are based on the daily maximum temperatures during 1981–2010. Blocking high events are defined as intervals in which daily 500-hPa geopotential height from the NCEP/NCAR reanalysis exceeds one standard deviation above the monthly mean for each grid cell over 5 consecutive days [41,44].

### SUPPLEMENTARY DATA

Supplementary data are available at [NSR](#) online.

### FUNDING

This work was supported by the National Key R&D Program of China (2016YFA0600703) and the National Natural Science Foundation of China (41875118, 41505073 and 41605059).

### AUTHOR CONTRIBUTIONS

S.H. designed the study. H.L. and C.W. provided the quantitative estimation of the energy input from the solar wind into Earth's magnetosphere. S.H. performed all the analysis and plotted the figures. S.H. wrote the initial manuscript, with input from H.W., F.L., H.L. and C.W.

**Conflict of interest statement.** None declared.

### REFERENCES

- Herschel W. Observations tending to investigate the nature of the Sun, in order to find the causes or symptoms of its variable emission of light and heat; with remarks on the use that may possibly be drawn from solar observations. *Int J Climatol* 1801; **91**: 85–9.
- Willson RC and Hudson HS. The Sun's luminosity over a complete solar cycle. *Nature* 1991; **351**: 42–4.
- Camp CD and Tung KK. Surface warming by the solar cycle as revealed by the composite mean difference projection. *Geophys Res Lett* 2007; **34**: L14703.
- Lean J. Solar ultraviolet irradiance variations: A review. *J Geophys Res-Atmos* 1987; **92**: 839–68.
- Labitzke K and Van Loon H. Associations between the 11-year solar cycle, the QBO and the atmosphere. Part I: The troposphere and stratosphere in the northern hemisphere in winter. *J Atmos Terr Phys* 1988; **50**: 197–206.
- Loon HV and Labitzke K. Association between the 11-year solar cycle, the QBO, and the atmosphere. Part II: Surface and 700 mb in the Northern Hemisphere in winter. *J Clim* 1988; **1**: 905–20.
- Labitzke K and Van Loon H. The signal of the 11-year sunspot cycle in the upper troposphere-lower stratosphere. *Space Sci Rev* 1997; **80**: 393–410.
- Frederick JE and Tinsley BA. The response of longwave radiation at the South Pole to electrical and magnetic variations: links to meteorological generators and the solar wind. *J Atmos Sol-Terr Phys* 2018; **179**: 214–24.
- Frederick JE. An analysis of couplings between solar activity and atmospheric opacity at the South Pole. *J Atmos Sol-Terr Phys* 2017; **164**: 97–104.
- Frederick JE. Solar irradiance observed at Summit, Greenland: possible links to magnetic activity on short timescales. *J Atmos Sol-Terr Phys* 2016; **147**: 59–70.
- Gray LJ, Rumbold ST and Shine KP. Stratospheric temperature and radiative forcing response to 11-year solar cycle changes in irradiance and ozone. *J Atmos Sci* 2009; **66**: 2402–17.
- Haigh JD. The role of stratospheric ozone in modulating the solar radiative forcing of climate. *Nature* 1994; **370**: 544–6.
- Gray LJ, Scaife AA and Mitchell DM *et al.* A lagged response to the 11 year solar cycle in observed winter Atlantic/European weather patterns. *J Geophys Res-Atmos* 2013; **118**: 13405–20.
- Mitchell D, Gray LJ and Fujiwara M *et al.* Signatures of naturally induced variability in the atmosphere using multiple reanalysis datasets. *Q J R Meteorol Soc* 2015; **141**: 2011–31.
- Crooks SA and Gray LJ. Characterization of the 11-year solar signal using a multiple regression analysis of the ERA-40 dataset. *J Climate* 2005; **18**: 996–1015.
- Frame TH and Gray LJ. The 11-yr solar cycle in ERA-40 data: an update to 2008. *J Clim* 2010; **23**: 2213–22.
- Holton JR. *An Introduction to Dynamic Meteorology*. New York: Academic Press, 3rd edn. 1992.
- Gray LJ, Beer J and Geller M *et al.* Solar influences on climate. *Rev Geophys* 2010; **48**: RG4001.
- Thiéblemont R, Matthes K and Omrani N-E *et al.* Solar forcing synchronizes decadal North Atlantic climate variability. *Nat Commun* 2015; **6**: 8268.
- Calvo N and Marsh DR. The combined effects of ENSO and the 11 year solar cycle on the Northern Hemisphere polar stratosphere. *J Geophys Res-Atmos* 2011; **116**: D23112.
- Zhou Q, Chen W and Zhou W. Solar cycle modulation of the ENSO impact on the winter climate of East Asia. *J Geophys Res-Atmos* 2013; **118**: 5111–9.
- Huth R, Bochníček J and Hejda P. The 11-year solar cycle affects the intensity and annularity of the Arctic Oscillation. *J Atmos Sol Terr Phys* 2007; **69**: 1095–109.
- Chen W and Zhou Q. Modulation of the Arctic Oscillation and the East Asian winter climate relationships by the 11-year solar cycle. *Adv Atmos Sci* 2012; **29**: 217–26.
- Kodera K and Kuroda Y. A possible mechanism of solar modulation of the spatial structure of the North Atlantic Oscillation. *J Geophys Res-Atmos* 2005; **110**: D02111.

25. He S-P, Wang H-J and Gao Y *et al.* Influence of solar wind energy flux on the interannual variability of ENSO in the subsequent year. *Atmos Ocean Sci Lett* 2018; **11**: 165–72.
26. Troshichev O, Egorova L and Janzhura A *et al.* Influence of the disturbed solar wind on atmospheric processes in Antarctica and El-Niño Southern Oscillation (ENSO). *Memorie-Societa Astronomica Italiana* 2005; **76**: 890–8.
27. Akasofu S-I. Energy coupling between the solar wind and the magnetosphere. *Space Sci Rev* 1981; **28**: 121–90.
28. Newell PT, Sotirelis T and Liou K *et al.* Pairs of solar wind–magnetosphere coupling functions: combining a merging term with a viscous term works best. *J Geophys Res-Space* 2008; **113**: A04218.
29. Li H, Wang C and He S-P *et al.* Plausible modulation of solar wind energy flux input on global tropical cyclone activity. *J Atmos Sol-Terr Phys* 2018; **192**: 104755.
30. Wang C, Han J and Li H *et al.* Solar wind–magnetosphere energy coupling function fitting: results from a global MHD simulation. *J Geophys Res-Space* 2014; **119**: 6199–212.
31. GISTEMP Team. GISS surface temperature analysis (GISTEMP). *NASA Goddard Institute for Space Studies*. Land-Ocean Temperature Index, ERSSTv5, 1200 km smoothing. New York: National Aeronautics and Space Administration; 2016.
32. Sullivan A, Luo JJ and Hirst AC *et al.* Robust contribution of decadal anomalies to the frequency of central-Pacific El Niño. *Sci Rep* 2016; **6**: 38540.
33. Kodera K and Kuroda Y. Dynamical response to the solar cycle. *J Geophys Res-Atmos* 2002; **107**: 4749.
34. Cionni I, Eyring V and Lamarque JF *et al.* Ozone database in support of CMIP5 simulations: results and corresponding radiative forcing. *Atmos Chem Phys* 2011; **11**: 11267–92.
35. Hartmann DL, Wallace JM and Limpasuvan V *et al.* Can ozone depletion and global warming interact to produce rapid climate change? *Proc Natl Acad Sci USA* 2000; **97**: 1412–7.
36. Charney JG and Drazin PG. Propagation of planetary-scale disturbances from the lower into the upper atmosphere. *J Geophys Res* 1961; **66**: 83–109.
37. Andrewes DG, Holton JR and Leovy CB. *Middle Atmosphere Dynamics*. San Diego: Academic Press, 1987.
38. He S, Wang H and Gao Y *et al.* Recent intensified impact of December Arctic Oscillation on subsequent January temperature in Eurasia and North Africa. *Clim Dyn* 2019; **52**: 1077–94.
39. Butchart N, Scaife AA and Bourqui M *et al.* Simulations of anthropogenic change in the strength of the Brewer–Dobson circulation. *Clim Dyn* 2006; **27**: 727–41.
40. Weber M, Dikty S and Burrows JP *et al.* The Brewer-Dobson circulation and total ozone from seasonal to decadal time scales. *Atmos Chem Phys* 2011; **11**: 11221–35.
41. Li F, Orsolini YJ and Wang H *et al.* Atlantic multidecadal oscillation modulates the impacts of Arctic sea ice decline. *Geophys Res Lett* 2018; **45**: 2497–506.
42. Kalnay E, Kanamitsu M and Kistler R *et al.* The NCEP/NCAR 40-year reanalysis project. *Bull Am Meteorol Soc* 1996; **77**: 437–71.
43. He S and Wang H. Linkage between the East Asian January temperature extremes and the preceding Arctic Oscillation. *Int J Climatol* 2016; **36**: 1026–32.
44. Thompson DW and Wallace JM. Regional climate impacts of the Northern Hemisphere annular mode. *Science* 2001; **293**: 85–9.